Croatian Society for Materials Protection

Metalurgija/Metallurgy

Vol. 66 No. 1 / 2027

Numerical Analysis of the Sensitivity of Maximum Impact Force to Parameter Variations in the Drucker–Prager Failure Model for Pneumatic Rock Drilling

Jianbing Pei [1], Dongfang Li [1*], Ming'an Zhou [1], Huiyi Zhu [1], Fangzan Luo [1], Zengyang Huang [2], Wentao Fu [3], Haibin Lin [3], Sufen Wang [4], Lichun Zhou [5]

https://doi.org/10.64486/m.66.1.9

[1] Quzhou College of Technology, Quzhou 324000, China; 21616733@qq.com; ldfqzy001@163.com; zhoumingan_zjqz@163.com; 279049166@qq.com; 5232242@qq.com
[2] Quzhou Intellectual Property Protection Center, Quzhou 324000, China; 897581793@qq.com
[3] Quzhou Academy of Metrology and Quality Inspection, Quzhou 324000, China; 312887541@qq.com; linhaibin_zj@163.com
[4] College of Mechanical Engineering, Quzhou University, Quzhou 324000, China; wangsufen09@163.com
[5] Yangtze Delta Region Institute (Quzhou), University of Electronic Science and Technology of China, Quzhou 324000, China; zhoulichun@csj.uestc.edu.cn
[*] Correspondence: ldfqzy001@163.com

Type of the Paper: Article
Received: April 23, 2026
Accepted: June 22, 2026

Abstract: This study investigates the rock-breaking process of pneumatic rock drills using the Drucker–Prager (D–P) strength criterion. A numerical drilling model comprising a rigid impact piston, a rigid drill bit, and D–P rock material was developed in ANSYS LS-DYNA. A sensitivity analysis was performed to evaluate the influence of key material parameters on the maximum impact force between the drill bit and rock. Mesh independence was confirmed with an optimal rock element size of 1.000 mm. The effects of maximum principal strain at failure, rock density, elastic shear modulus, Poisson's ratio, friction angle, dilation angle, and cohesion were examined over a variation range of ±10 % to ±50 %. Results show that the elastic shear modulus has the strongest influence on the maximum impact force, exhibiting an approximately linear positive relationship. The maximum principal strain at failure also significantly affects impact force, whereas density and Poisson's ratio produce non-monotonic responses. Friction and dilation angles show strong sensitivity within a limited angular range, while cohesion has only a minor effect. Furthermore, the elastic shear modulus remains the dominant parameter even under different failure-strain conditions, indicating an interaction between stiffness and failure characteristics. The findings provide guidance for predicting drilling forces, optimizing drill-bit design, and improving drilling efficiency through better matching of rock properties and drilling parameters.

Keywords: pneumatic rock drilling; Drucker–Prager criterion; finite element modelling; sensitivity analysis; impact force; rock fragmentation

1. Introduction

As one of the most commonly used rock breaking tools in geotechnical engineering, impact rock breaking efficiency and mechanisms of pneumatic rock drills are important in improving rock breaking performance and optimizing essential components. Impact rock breaking under dynamic loading is mechanically changing rock damage, crack propagation and crushing zone formation. With the rapid advances in rock mechanics theory and numerical simulation technology, impact rock breaking research has evolved from empirical description to a theoretical and model-based approach. H. Cheng et al. [1] found that rock in dynamic loading typically undergoes phases of compaction, elastic deformation, plastic yield, failure, and residual strength. The mechanical behaviour of rock is quite different under dynamic and static loading conditions. In addition, increasing loading rate increases dynamic strength and shear modulus of rock. Also, the failure mode changes from progressive failure under static loading to brittle fracture under dynamic loading. T. Hu et al. [2] showed that the bedding structure of carbonaceous slate influences the failure mode. Under dynamic impact, initial cracks start in areas of stress concentration and propagate along the direction of maximum tensile stress. C. Huang [3] selected the D-P failure criterion in conjunction with rock breaking mechanisms, divided the rock breaking area, and established a blasting analysis model. He also studied failure factors. The results showed that the calculation model of blasting rock breaking range based on the D-P failure criterion predicted crushing zone, fracture zone, and fracture propagation zone extents.

Y. Li [4] investigated a weak-strong discontinuous coupling numerical method for strain localization problems and progressive failure of rock masses. He assessed the stability and simulation performance of the finite element numerical method. Parameter determination and model verification remained heavily dependent on experiments, and there was no general cross-scale prediction method. Further experiments and multi-scale simulations were needed to establish a parameter database and identification method. T. Saksala [5] et al. proposed a damage-viscoplastic model of granite failure using the D-P model for shear failure and the modified Rankine model for tensile failure, bit-rock contact model, penalty function method, and bit-rock contact model. Bit was simplified as a rigid body model. The model captured asymptotic failure of rock in frictional sliding by using separate tensile-compressive damage variables. The model was validated by a uniaxial tension-compression test. The model does not have an element deletion algorithm. It does not simulate the actual evolution of cuttings formation and rock pits on the rock surface. G. Sansyzbekov et al. [6] investigated crack propagation in granite at temperatures from 25 °C to 800 °C and its effects on physical and mechanical properties. It reported significant changes in parameters such as porosity, wave velocity, tensile strength and elastic modulus obove 600 °C. Results suggested a link between crack propagation and macroscopic properties. Notwithstanding, no quantitative mapping relationship between geometric features and distribution pattern of microcracks and macroscopic mechanical response was established.

M. Pressacco [7] et al. conducted numerical simulations to explore how microwave irradiation weakens the mechanical properties of rock, indicating that microwave pretreatment significantly decreases the uniaxial compressive strength and tensile strength of rocks, but did not consider thermoplastic deformation during microwave irradiation and crack response to electromagnetic fields. X. Wang et al. [8] developed an elastic-plastic analytical model based on the elastic zone, plastic softening zone and fractured zone with elastic zone, plastic softening zone and fractured zone. Models took into account intermediate principal stress, strain softening and rock mass dilation based on the D-P criterion and the non-associated flow rule. They verified model effectiveness and examined impact parameters such as residual strength, in-situ stress, and support strength on surrounding rock stress, displacement and the extent of the plastic zone. Their results provided a theoretical basis for support design, but they did not consider systematic analysis of the model grid size. H. Liu et al. [9] computed the boundary equation of the plastic zone in the surrounding rock of the roadway using D-P criteria and a 3D stress field, and studied the effect of horizontal and axial lateral pressures on the shape and size of the plastic zone. They believed that axial lateral pressures primarily affect the size of the plastic zone. There are significant differences in the results of the plastic zone calculation for different D-P criteria, the most conservative one being the circle criterion DP-3. However, there are no clear physical mechanism explanations or on-site empirical support to match specific criteria with the geological and stress environment. Calculations for different criteria vary considerably, and the selection of criteria in engineering remains subject to engineering experience, and there is no unified standard.

 https://doi.org/10.64486/m.66.1.9

Q. Xia et al. [10] compared existing three-dimensional strength theories in geotechnical engineering and studied the formation of strength theory and the earth pressure calculation framework, proposed and developed the twin-shear unified strength theory, D-P series criteria for intermediate principal stress and earth pressure model, development of plastic zone of surrounding rock under 3D stress field and examples. Although significant progress in 3D strength theory and stress analysis has been made, the physical mechanism and determination method for the influence coefficient b of the intermediate principal stress remain unclear. Y. Xue et al. [11] combined strength theory and energy theory, taking into account practical factors such as rock mass integrity and weathering degree, and proposed a damage factor for rock mass deterioration. By considering rock mass integrity coefficient, weathering coefficient and damage factor, they proposed solution formulas for cohesion and internal friction angle, and developed a complete determination method for rockburst grade with improved Mohr-Coulomb (M-C) and D-P strength criteria. They proposed a three-stage progressive rockburst mechanism with "yield, damage and energy release".

To sum up, the mechanism of the intermediate principal stress remains unclear. In summary, the finite element analysis of the maximum impact force between the drill bit and rock was used to analyze the sensitivity of the parameter variations of rock failure model. The rock breaking process of the equipment was studied, and the drilling force was calculated. This work helps design an optimal drilling equipment system, and provides a basis for further research on stiffness-adaptive drilling performance and control strategies for rock drilling.

2. Establishment of numerical analysis model for drilling force and explanation of size independence of the finite-element mesh division

2.1. Establishment of numerical analysis model

The impact of a pneumatic rock drill bit on rock involves stress wave propagation, energy conversion and dynamic rock fracture. Compressed air drove the piston to reciprocate at high speed in the cylinder. At the moment of impact, the piston hit the drill bit, and after reaching the maximum velocity, the piston functioned as the pressure energy of compressed air turned into the energy of the piston. Ideal conditions and without plastic deformation would be considered as an approximately elastic collision in which momentum and energy are transferred between the piston and drill bit. The impact of the piston hitting the drill bit produces a very small compressive stress pulse of very short duration (usually several hundred microseconds) at the top end of the drill bit and this stress wave propagates along the drill pipe towards the rock at the speed of sound, carrying most of the energy of impact and with high energy density. Compared to rock, the piston and drill bits are much stiffer. In the model of the drilling system using ANSYS LS-DYNA software, the piston and drill bit are simplified as rigid bodies, and rock is represented using the D-P constitutive material model [12–17], and the definition of internal friction angle P_{HI} under true triaxial strength condition is shown in Figure 1. The D-P strength criterion, proposed by Drucker et al. in 1952, was developed as an extension of the von Mises yield criterion. It is the theory that the material would suffer damage if the shear stress on the octahedral plane of the spatial stress reached a certain critical value [14]:

$$\alpha I_1 + \sqrt{J_2} - k = 0 \tag{1}$$

where, α and k are material parameters related only to the angle of friction of rock P_{HI} and cohesion value of rock C_{VAL}. The specific expressions of these parameters can be found in Refs. [10–16]. I_1 is the sum of the principal stress whose expression is:

$$I_1 = \sigma_x + \sigma_y + \sigma_z = \sigma_1 + \sigma_2 + \sigma_3 \tag{2}$$

J_2 is the second invariant of the stress deviator whose expression is:

$$J_2 = \frac{1}{6}[(\sigma_x - \sigma_y)^2 + (\sigma_y - \sigma_z)^2 + (\sigma_z - \sigma_x)^2] + \tau_{xy}^2 + \tau_{yz}^2 + \tau_{zx}^2 \tag{3}$$

https://doi.org/10.64486/m.66.1.9

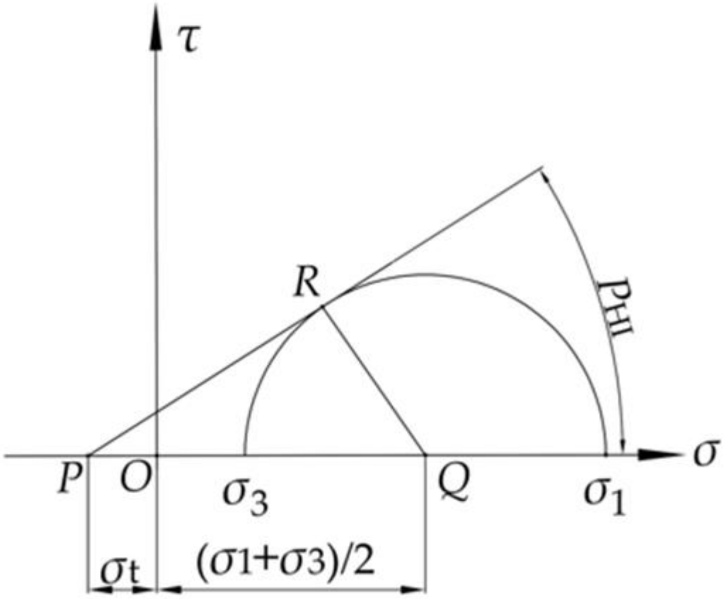

Figure 1. Definition of internal friction angle P_{HI} under true triaxial strength condition

The yield surface of the D-P strength criterion in the principal stress space is smooth [14], which makes it useful for numerical calculations. Therefore, the D-P strength criterion is widely used for numerical analysis of rock mechanics and engineering.

Many material constitutive models are not permitted to fail or erode. To simulate material failure, it was necessary to manually add a failure mode. The *MAT_ADD_EROSION option provided a failure model suitable for simulation of failure of rock materials. In this paper, element failure was obtained by defining the maximum principal strain at failure ε_{max} [12].

In order to simplify modeling, rock pores and temperature during drilling [12] and drill bit wear were not considered [13]. To maintain contact between the bit and the rock during impact drilling, a certain axial drilling pressure is required [16–19]. In this study, the drilling axial pressure was set to 9 kN, the impact velocity is 7.37 m/s, the rotary speed is 15 rpm, and the impact frequency is 14 Hz.

The characteristics of the rock model material [12] are shown in Table 1, and the three-dimensional finite-element model of the drilling is shown in Figure 2.

Table 1. The characteristics of the rock model material

No.	Variable	Value
1	mass density of rock, r_o / kg/m^3	2530
2	elastic shear modulus of rock, G_{MOD} / 10^3 MPa	7.4167
3	Poisson ratio of rock, R_{nu}	0.2
4	elasticity modulus of rock, E / MPa	17.8 × 10^3
5	angle of friction of rock, P_{HI} / °	45
6	dilation angle of rock, P_{SI} / °	45
7	cohesion value of rock, C_{VAL} / 10^6 Pa	19.2

https://doi.org/10.64486/m.66.1.9

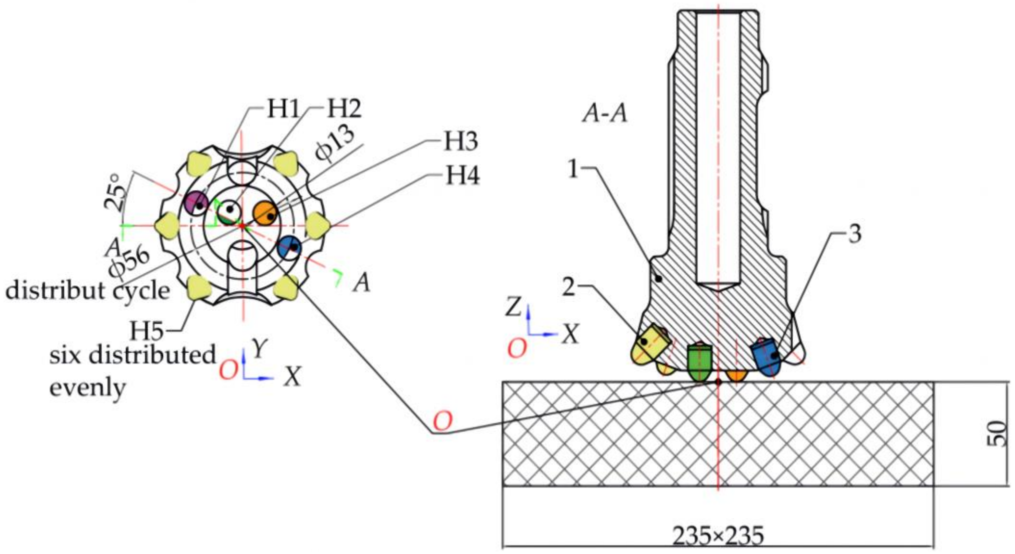

1-Drill bit; 2-Column tooth H1-H4 (4-φ13 mm × 19 mm); 3-Column tooth H5 (φ14 mm × 22 mm, six distributed evenly)

(a) Drilling structure model (impact piston was not shown)

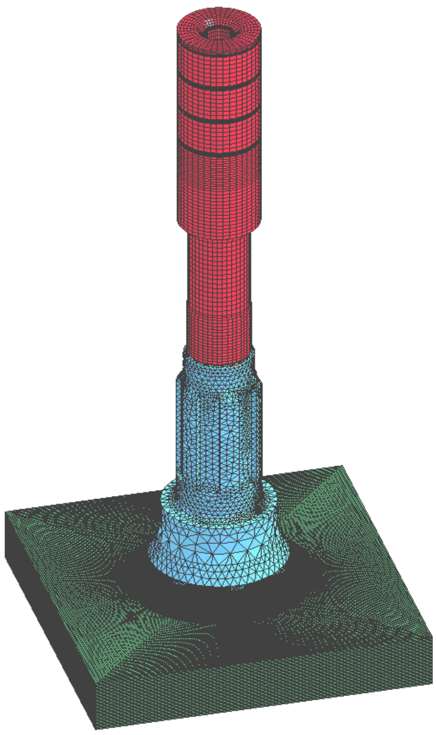

(b) Drilling finite-element model (impact piston was shown)

Figure 2. Schematic diagram of drilling structure and finite-element model

2.2 Mesh Size Independence Analysis

The refinement size of rock modeling directly impacts numerical results. Therefore, a mesh-independence analysis was performed to evaluate the influence of element size on the numerical results. Models with rock modeling refinements of 0.700 mm, 0.750 mm, 0.850 mm, 0.875 mm, 0.925 mm, 0.975 mm, 1.000 mm, 1.050 mm, 1.075 mm, 1.125 mm and 1.250 mm were chosen for calculation and the maximum drilling force between the drill bit and rock, F_{tlmax}, was extracted.

https://doi.org/10.64486/m.66.1.9

The curve is shown in Figure 3.

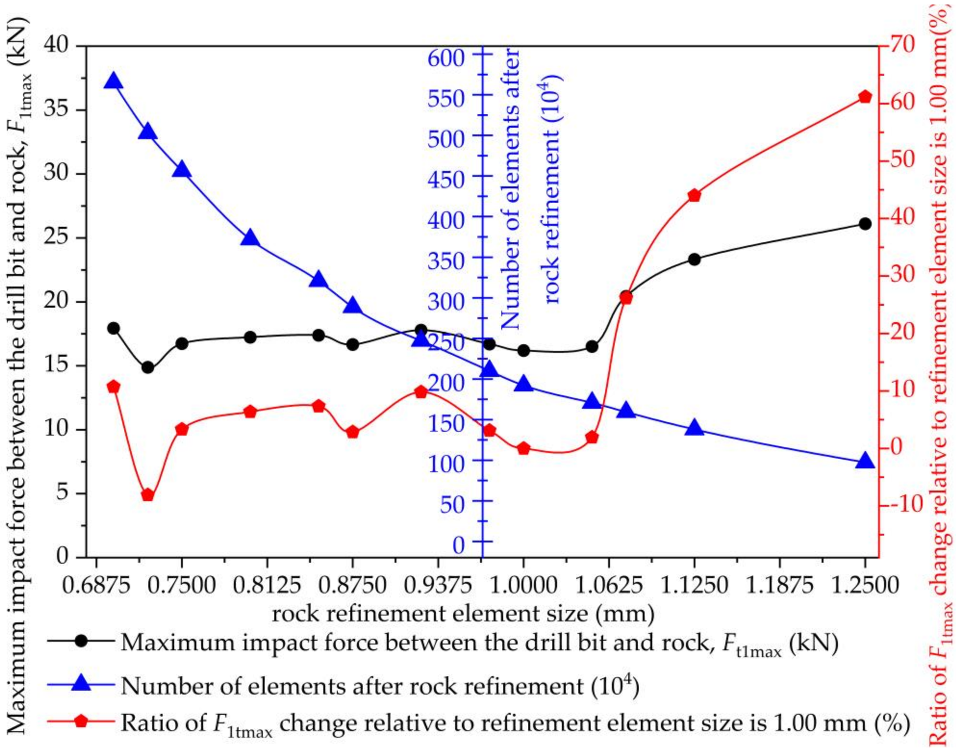

Figure 3. The distribution of maximum impact force between the drill bit and rock F_{tlmax} under different rock refinement element sizes

It shows that when rock modeling refinements ranged from 0.750 mm to 1.050 mm, F_{tlmax} ranged from 16.20 kN to 17.79 kN with a relative change rate between -66.08 % to 6.74 %. Specifically, for rock refinement sizes ranging from 0.975 mm to 1.050 mm, the corresponding F_{tlmax} value varies between 16.20 kN and 16.70 kN, and the relative variation does not exceed 3.12 %. Hence, the rock element size can be chosen within the interval of 0.975 mm to 1.050 mm. Unless otherwise stated, all subsequent rock models adopt a uniform size of 1.000 mm. This indicates relative stability and meets the accuracy requirements for engineering analysis. Further, the number of rock division units decreased dramatically with increasing rock modeling refinement size. For example, at 0.725 mm rock modeling refinement size scale was 502.7 × 104. At rock modeling refinement size of 1.000 mm scale decreased to 192.1 × 104, which implies a relative decrease of 61.80 %. This greatly reduces simulation computation time and computing hardware requirements. Therefore, after careful evaluation, a rock element size of 1.000 mm was selected for all subsequent simulations.

2.3 Numerical analysis results of drilling process

The drilling process was simulated using the developed finite-element model. Figure 4 shows the evolution of surface damage propagation in the rock at three representative stages during percussive drilling. The selected time intervals illustrate the initiation, expansion and development of the damaged zone under repeated impacts of the drill bit.

https://doi.org/10.64486/m.66.1.9

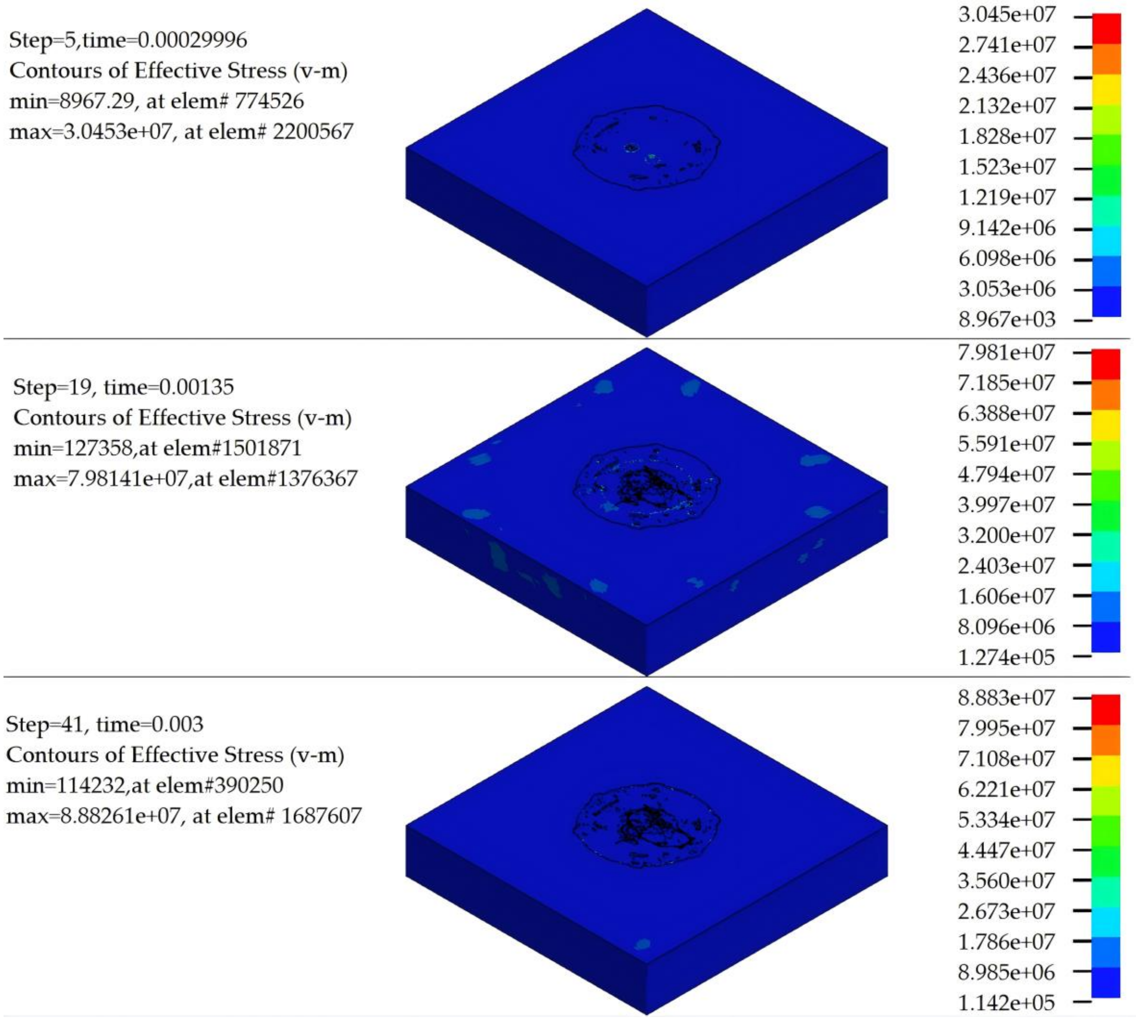

Figure 4. Evolution of surface damage propagation in rock under percussive drilling at selected time interval

At 0.00029996 s, column teeth H2 and H3 are first tapped by the shock wave, creating damage pits, which shows that the formation of damage pits by the "initial impact" of the H2 and H3 column teeth is irreplaceable. By 0.00135 second, six equally spaced H5 column teeth begin to break the rock. After that, at 0.003 second, the damage surface expands and a larger damage surface is formed. The reciprocating piston forces the drill bit to hit the rock surface repeatedly, and the borehole diameter gradually increases. The debris is removed by compressed air through holes in the drill bit.

3. The distribution of maximum impact force between the drill bit and rock (F_{tlmax}) under maximum principal strain at failure (ε_{max}) variation

To evaluate the influence of the maximum principal strain at failure (ε_{max}) on the drilling response, a series of numerical simulations was performed by varying ε_{max} while keeping all other material parameters constant. The resulting maximum impact force between the drill bit and rock (F_{tlmax}) was extracted for each simulation case. The corresponding results are presented in Figure 5.

 https://doi.org/10.64486/m.66.1.9

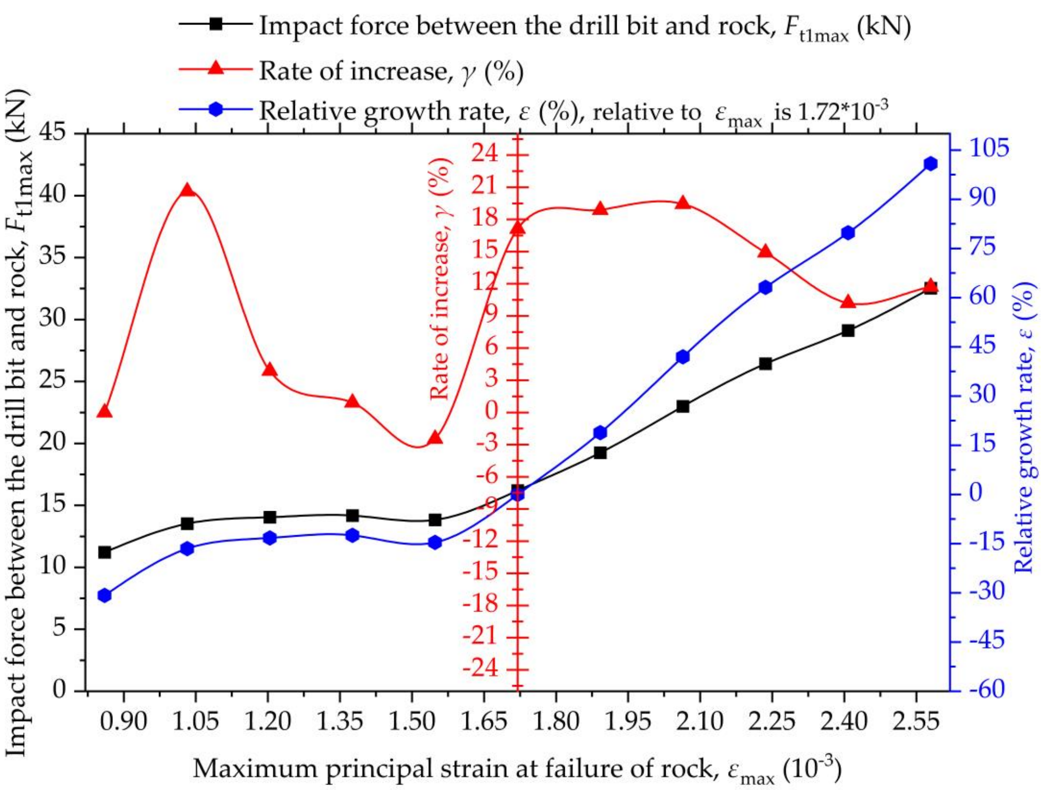

Figure 5. The distribution of F_{t1max} under ε_{max} variation

The study model is chosen to take the maximum principal strain at failure at ±10 %, ±20 %, ±30 %, ±40 %, and ±50 %. The maximum impact force between the drill bit and rock, F_{t1max}, is obtained and shown in Figure 5. Results show that F_{t1max} continues to grow as ε_{max} rose from 0.860 × 10^{-3} to 2.580 × 10^{-3} within -50 % to 50 % range. Growth rate decreases gradually, indicating that improving rock ultimate deformation capacity has a positive impact on load transmission effect, but decreases with strain level increasing. F_{t1max} grows steadily from 0.086 × 10^{-3} to 2.580 × 10^{-3}, and F_{t1max} continuously increases from 11.21 kN to 32.54 kN, with a steady growth rate. The growth rate varies with strain level. The relative growth rate ranges from -30.77 % to 100.87 %, suggesting changing F_{t1max} to variation of F_{t1max} variation with strain level. F_{t1max} played an important role in rock's ultimate plastic deformation capability before failure. Lower ε_{max} values (e.g., 0.086 × 10^{-3} to 1.548 × 10^{-3}) rock is brittle, leading to concentrated impact energy on local crack propagation and relatively low F_{t1max} values (from 11.21 kN to 14.18 kN).

However, as ε_{max} increased (e.g., beyond 1.72 × 10^{-3}), the rock's ductility improved, enabling it to absorb more impact energy and dissipate it over a broader range of plastic deformation. This led to an almost linear increase in F_{t1max} necessary for inducing macroscopic fragmentation.

4. Effect of variation of constitutive characteristic parameters of the D-P materials on the distribution of maximum impact force between the drill bit and rock (F_{t1max})

For most analysis of system stability, we perform sensitivity analysis [20–22]. In this analysis, we first specified the baseline parameters. When considering the effect of a change in a parameter on the objective function, baseline values of the other parameters are the same. If a small change in a parameter leads to a significant change in the objective, it indicates that the objective is sensitive to this parameter; if the objective changes little, it indicates that the objective is not sensitive to this parameter.

 https://doi.org/10.64486/m.66.1.9

4.1 The distribution of F_{tlmax} under mass density of rock (r_o) variation

To evaluate the influence of rock mass density (r_o) on the drilling response, a parametric study was conducted by varying the density while keeping all other material parameters constant. The resulting variation of the maximum impact force between the drill bit and rock (F_{tlmax}) is shown in Figure 6.

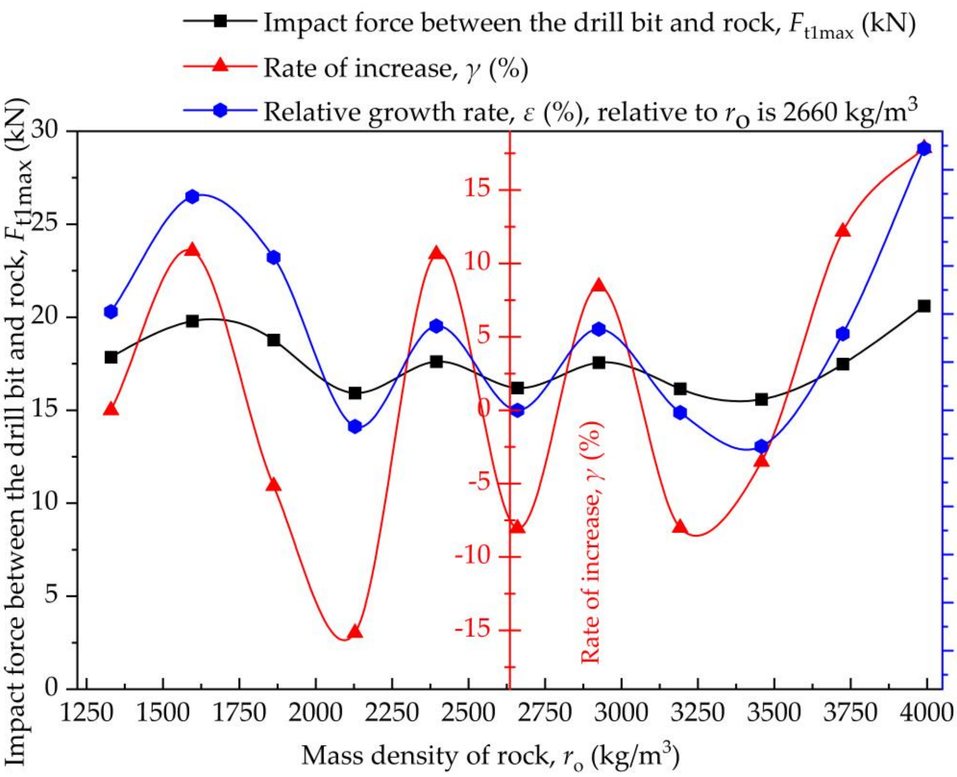

Figure 6. The distribution of F_{tlmax} under r_o variation

The density variation of the D-P constitutive model was chosen from ±10 %, ±20 %, ±30 %, ±40 % and ±50 %. The maximum impact force between the drill bit and rock, F_{tlmax}, is obtained and shown in Figure 6. The results showed that in the range -50 % to 50 % (an increase in density from 1265 kg/m^3 to 3795 kg/m^3) F_{tlmax} has an overall fluctuating upward trend with a change rate between -3.75 % to 27.21 %. In particular, when the density increases from 1518 kg/m^3 to 2024 kg/m^3, F_{tlmax} drops from 19.79 kN to 15.93 kN. Conversely, when the density increases from 3542 kg/m^3 to 3795 kg/m^3, F_{tlmax} rises from 17.49 kN to 20.61 kN. The growth rate of Ftlmax shows a significant variation, suggesting that the influence of r_o on F_{tlmax} exhibited stage characteristics. The r_o value of the rock affected its inertial mass and wave impedance, changing the propagation and reflection characteristics of stress waves at the drill bit and rock interface. An increase in r_o will tend to increase the inertial resistance of the rock. Changes of r_o cause waves with impedance mismatch and the transmission efficiency of impact energy decreases, leading to a decrease in F_{tlmax}. The differences in r_o also affect plastic yielding and hardening behavior of rock. This affects energy dissipation during impact. Lower values of r_o make rock more plastic and absorb some impact energy. Higher values of r_o increase rock stiffness and convert more impact energy into crushing work which causes F_{tlmax} to increase. The non-monotonic variation of F_{tlmax} is due to the stress wave superposition effect of rock under certain r_o conditions and boundary conditions.

4.2 The distribution of F_{tlmax} under elastic shear modulus of rock (G_{MOD}) variation

To investigate the influence of the elastic shear modulus of rock (G_{MOD}) on the drilling response, a parametric analysis was performed by varying G_{MOD} while maintaining all other material parameters unchanged. The resulting variation of the maximum impact force between the drill bit and rock (F_{tlmax}) is presented in Figure 7.

 https://doi.org/10.64486/m.66.1.9

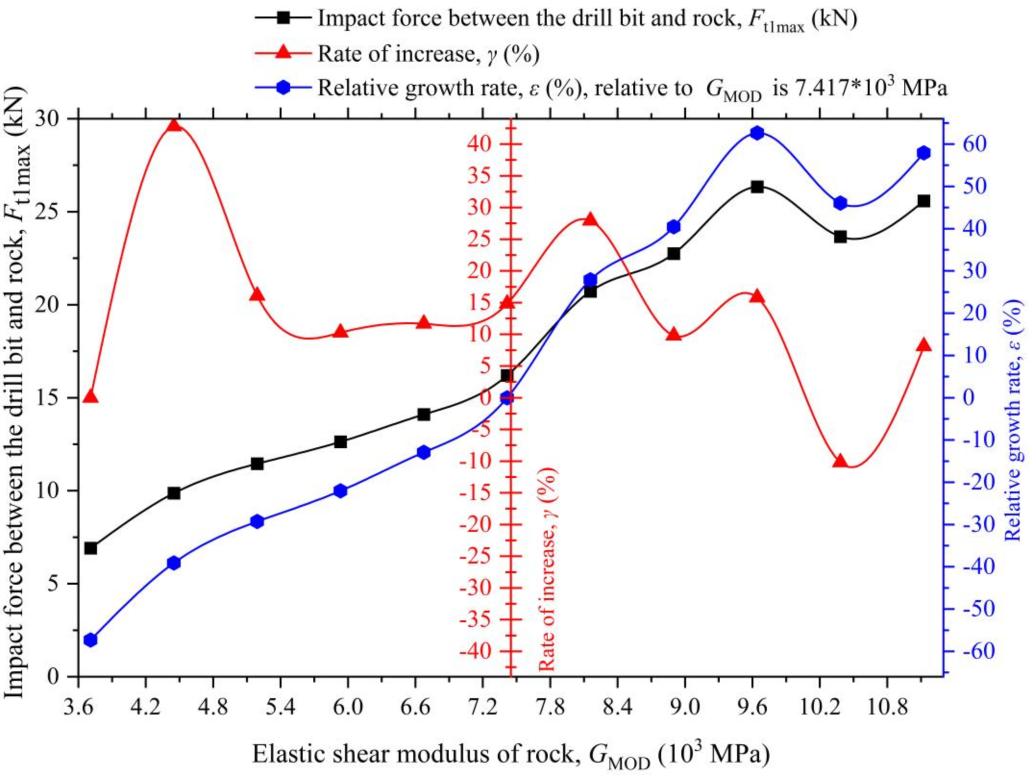

Figure 7. The distribution of F_{tlmax} under G_{MOD} variation

Models with variations in the elastic shear modulus of rock G_{MOD} in the D-P model at ±10 %, ±20 %, ±30 %, ±40 % and ±50 % and the maximum impact force between the drill bit and rock, F_{tlmax}, is obtained and shown in Figure 7. Results showed that in the range from -50 % to 50 % variation range (G_{MOD} increasing from 3.708 × 10^3 MPa to 11.125 × 10^3 MPa), F_{tlmax} increased nearly linearly with G_{MOD}. The change rate ranged from -57.33 % to 62.66 %. G_{MOD} increased from 3.708 × 10^3 MPa to 11.125 × 10^3 MPa, F_{tlmax} increased from 6.91 kN to 25.58 kN, showing a constant increase overall but with some fluctuations in growth rate. When G_{MOD} increased from 3.708 × 10^3 MPa to 5.192 × 10^3 MPa, F_{tlmax} increased from 6.91 kN to 11.46 kN (growth rate 16.81 %) and then increased from 8.900 × 10^3 MPa to 9.642 × 10^3 MPa, F_{tlmax} increased from 22.75 kN to 26.35 kN with a growth rate of 15.81 % (growth rate decreased significantly from the previous phase (G_{MOD} increasing from 7.417 × 10^3 MPa to 8.158 × 10^3 MPa, resulting in a 27.92 % rise in maximum rock drilling force). Lower G_{MOD} indicates soft rocks, which absorb more energy from plastic deformation, and thus smaller F_{tlmax}. With increasing G_{MOD}, rock stiffness increases, stress wave propagation speed increases, energy transfer efficiency increases, and F_{tlmax} increases strongly. For example, at 11.125 × 10^3 MPa, F_{tlmax} reached 25.58 kN. Nonlinear changes in F_{tlmax} growth rates are associated with wave impedance matching states of rocks under stiffness conditions. When G_{MOD} increased in a specific range (for example, from 7.417 × 10^3 MPa to 8.158 × 10^3 MPa), F_{tlmax} growth is phased up, increasing from 16.20 kN to 20.72 kN (with a growth rate of 27.92 %). Stress wave reflection decreases, resulting in better energy coupling between the drill bit and rock interface. When G_{MOD} reached relatively high levels, F_{tlmax} growth rate decreased due to reflection of some of the impact energy due to rock stiffness and lower energy absorption efficiency.

4.3 The distribution of F_{tlmax} under Poisson ratio of rock (R_{nu}) variation

The analysis models were selected with variations in the Poisson ratio of rock (R_{nu}) in the D–P constitutive model, while all other parameters were kept constant. The resulting maximum impact force between the drill bit and rock (F_{tlmax}) was obtained and is shown in Figure 8.

 https://doi.org/10.64486/m.66.1.9

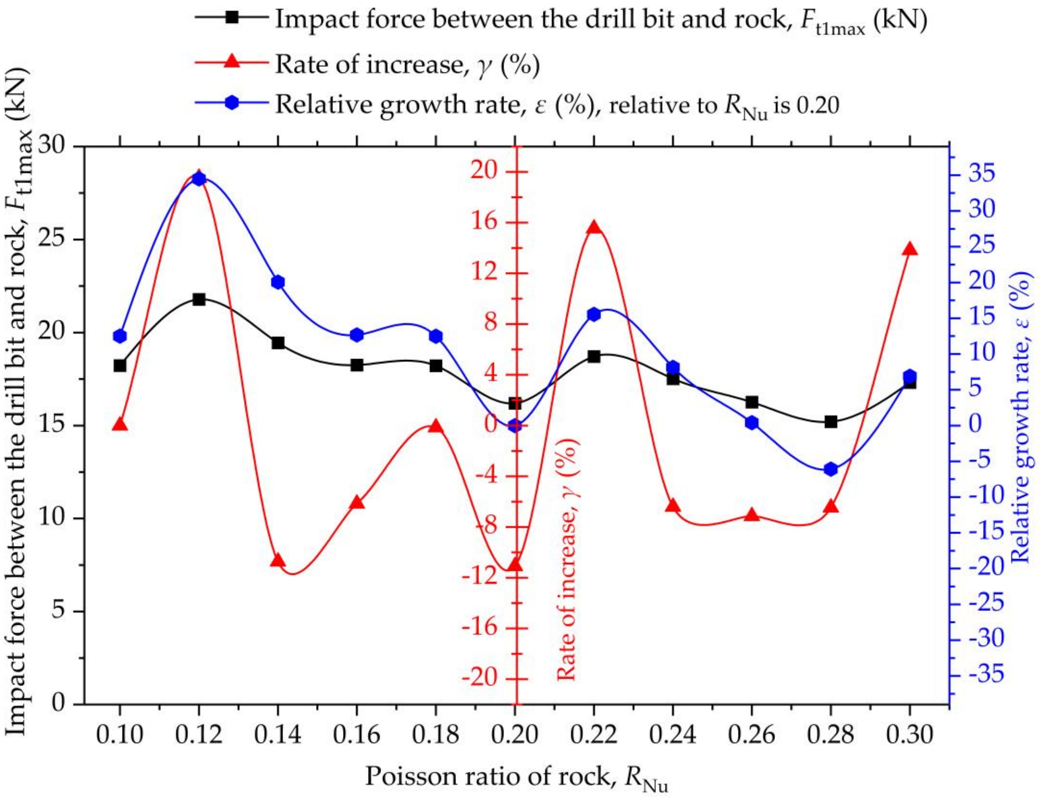

Figure 8. The distribution of F_{t1max} under R_{nu} variation

The analysis models were selected with the Poisson ratio of rock R_{nu} in the D-P constitutive model set at ±10 %, ±20 %, ±30 %, ±40 % and ±50 % for calculating the maximum impact force between the drill bit and rock F_{t1max}, shown in Figure 8. The results show that as the Poisson ratio R_{nu} increases from -50 % to 50 % (from 0.10 to 0.30), F_{t1max} varies non-monotonically, with local extremes -11.10 % to 19.53 % of changes. For example, as R_{nu} increases from 0.10 to 0.30, F_{t1max} initially increases and then decreases. At R_{nu} = 0.12, F_{t1max} peaks at 21.79 kN and drops to a minimum of 16.20 kN at R_{nu} = 0.20. A slight rebound occurs at R_{nu} = 0.22, reaching 18.72 kN and dropping to 15.21 kN at R_{nu} = 0.28. The growth rate of F_{t1max} and relative growth rate also fluctuated strongly. When R_{nu} increases from 0.10 to 0.12, γ is 19.53 %; whereas when R_{nu} increases from 0.12 to 0.14, γ drops to 10.73 %. The sensitivity turning point of F_{t1max} is observed around R_{nu} = 0.12. The R_{nu} directly affected the lateral deformation ability and volume response of rock. With a lower Poisson ratio, rock is more likely to contract under impact loading and stress local concentration, and cracks propagate. With further increases in R_{nu}, rock volume deformation constraint increased and impact energy dissipated in volume compression rather than local fragmentation, and F_{t1max} decreased gradually. In particular, as R_{nu} increased from 0.18 to 0.20, F_{t1max} decreased from 18.22 kN to 16.20 kN. At R_{nu} = 0.22, F_{t1max} briefly recovered to 18.72 kN due to rock being dynamically balanced between stress wave propagation and energy absorption at this R_{nu}. A Poisson's ratio of 0.3 is a typical value for rock and indicates moderate compressibility; an increase in Poisson's ratio leads to enhanced lateral confinement, thereby increasing the impact force.

4.4 The distribution of F_{t1max} under angle of friction (P_{HI}) and dilation angle of rock (P_{SI}) variation

To evaluate the combined influence of the angle of friction (P_{HI}) and dilation angle (P_{SI}) on the drilling response, a series of numerical simulations was performed by varying both parameters simultaneously while maintaining equal values of P_{HI} and P_{SI}. The resulting variation of the maximum impact force between the drill bit and rock (F_{t1max}) is presented in Figure 9.

https://doi.org/10.64486/m.66.1.9

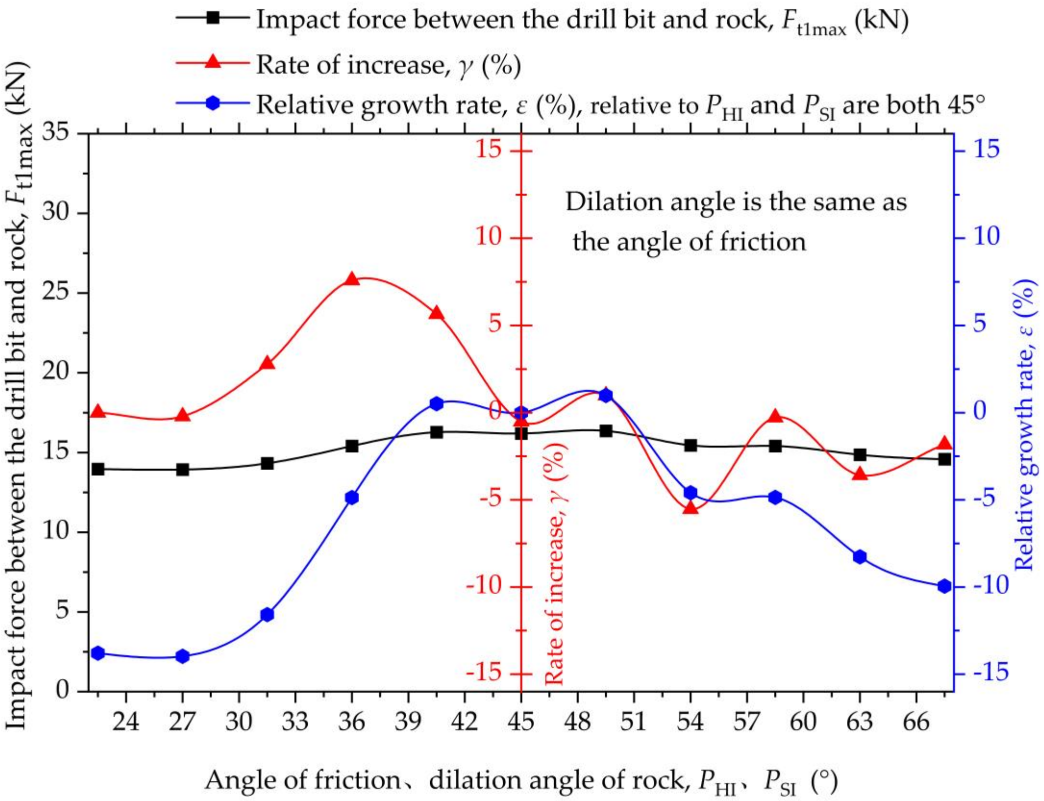

Figure 9. The distribution of F_{t1max} under P_{HI}, P_{SI} variation

The models with the ranges of the friction angle and dilation angle of rock P_{HI}, P_{SI} in the D-P constitutive model at ±10 %, ±20 %, ±30 %, ±40 % and ±50 % were used for calculation. The maximum impact force between the drill bit and rock, F_{t1max}, is obtained and shown in Figure 9. As the friction angle and dilation angle range from -50 % to 50 % (up to 22.5° to 67.5°), F_{t1max} stabilized in the lower angle range (up to 40.5°) and stabilized after 40.5°, with a change rate from -5.53 % to 7.79 %. This behavior shows the gradual impact of rock shear strength and volume deformation properties on energy transfer. The gradual increase of F_{t1max} from 13.90 kN to 16.36 kN as the friction angle and dilation angle increase from 22.5° to 67.5°, showed a non-linear growth process. Between 22.5° and 27°, F_{t1max} remained around 13.93 kN. From 27° to 40.5°, F_{t1max} increased continuously, but the range of increase was small, between 2.78 % and 7.59 %. From 40.5° to 49.5°, F_{t1max} slightly increased to 16.36 kN. From 49.5° to 67.5°, F_{t1max} decreases steadily to 14.59 kN. The friction angle and dilation angle control the shear strength and plastic volume strain of the rock. At lower angles, the rock has weak shear strength and plastic flow dominates. Further impact energy is dissipated as the rock weakens. As the angle increases, the shear strength and brittleness of the rock increase. Under impact loading, crack propagation becomes easier and more extensive. F_{t1max} is required to start the crushing process. F_{t1max} gradually increases from 13.93 kN to 16.28 kN. When the angle is small and steadily increases, the shear strength of the rock reaches its limit and stabilizes the crushing process. Additionally, increasing the dilation angle leads to a significant volume expansion effect. The internal frictional resistance and energy dissipation of the rock stabilize, so F_{t1max} remains stable after decreasing to a certain value.

4.5 The distribution of F_{t1max} under cohesion value of rock (C_{VAL}) variation

To investigate the influence of the cohesion value of rock (CVAL) on the drilling response, a parametric analysis was performed by varying CVAL while keeping all other material parameters constant. The resulting variation of the maximum impact force between the drill bit and rock (F_{t1max}) is presented in Figure 10.

https://doi.org/10.64486/m.66.1.9

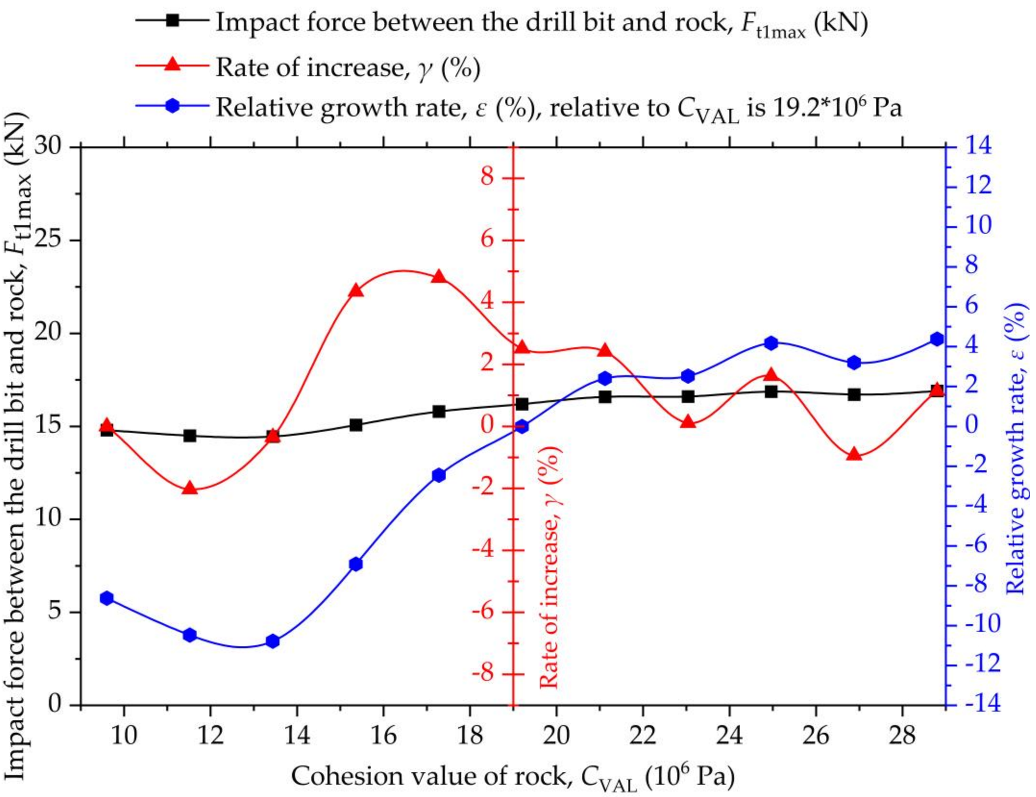

Figure 10. The distribution of maximum impact force between the drill bit and rock F_{tlmax} under the condition of cohesion value of rock C_{VAL} variation

In the analysis model, C_{VAL} changed in the D-P model ranges from ±10 % to ±50 %. The maximum impact force between the drill bit and rock, F_{tlmax}, was measured and shown in Figure 10. Results showed that the C_{VAL} changes from 9.6 MPa to 28.8 MPa had a slight upward trend from -50 % to 50 %. The overall sensitivity was low and that C_{VAL} changes only moderately on dynamic impact rock breaking force from -2.03 % to 4.69 % of the parameter range, with relative change rate between -2.03 % and 4.79 % of the parameter range. For example, the C_{VAL} change of 9.6 MPa to 28.8 MPa, F_{tlmax} fluctuated from 14.80 kN to 16.91 kN, making a small overall increase of about 14.23 % of the value. We note that F_{tlmax} variation was fluctuating rather than monotonic increase. When C_{VAL} changes from 21.12 MPa to 28.80 MPa, F_{tlmax} is stable between 16.59 kN and 16.91 kN, with change rate ranging from -0.94 % to 2.41 %. The relative growth rate of F_{tlmax} is low between 0.0 % and 4.38 %, which indicates that the maximum rock drilling force was not affected by changes in C_{VAL}. We found that C_{VAL} is the initial cohesive force between rock particles, which affects rock yield independent of hydrostatic pressure. The rock breaking effect was driven by stress wave propagation and reflection, and dynamic crack expansion at high strain rate. Unlike friction angle controls shear strength, C_{VAL} had little effect on dynamic strength. Hence F_{tlmax} was not affected.

4.6 The distribution of F_{tlmax} under elastic shear modulus of rock (G_{MOD}) with different maximum principal strain at failure (ε_{max})

To further investigate the interaction between the elastic shear modulus of rock (GMOD) and the maximum principal strain at failure (εmax), a series of numerical simulations was conducted by varying GMOD under different εmax conditions. The resulting variation of the maximum impact force between the drill bit and rock (F_{tlmax}) is presented in Figure 11.

 https://doi.org/10.64486/m.66.1.9

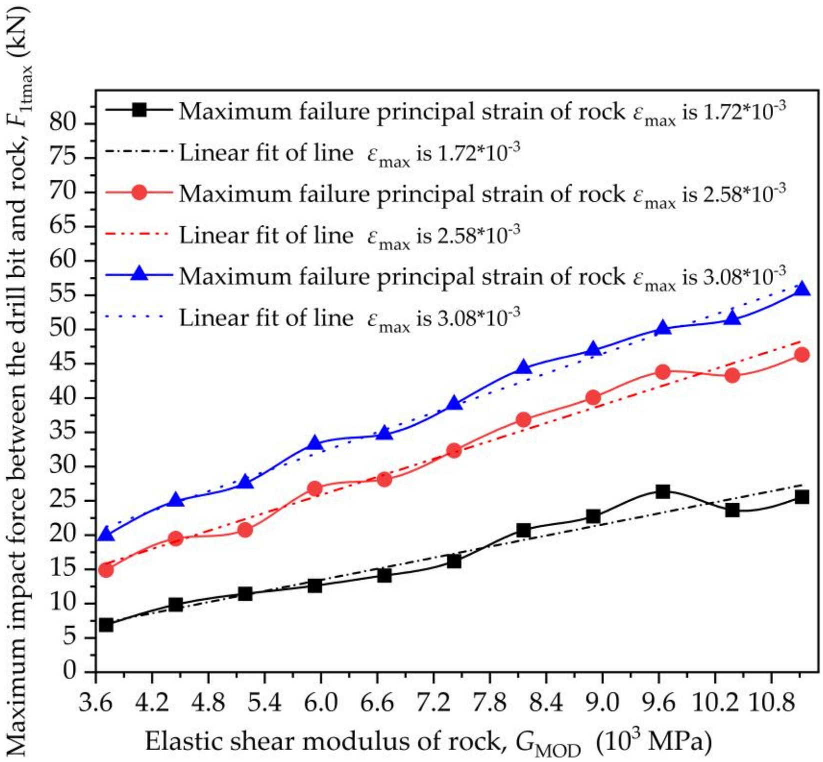

Figure 11. The distribution of F_{tlmax} under G_{MOD} with different ε_{max}

Previous analysis showed that rock G_{MOD} variation influences the maximum impact force distribution between the drill bit and rock, F_{tlmax}, distribution in the D-P rock material. Models with different rock G_{MOD} variations under different ε_{max} conditions were chosen for study. Models with different rock G_{MOD} variations ranging between 10 %, 20 %, 30 %, 40 % and 50 % in the D-P constitutive model were selected for calculation of F_{tlmax} distribution, shown in Figure 11. G_{MOD} distributions for different rock G_{MOD} variations under different ε_{max} conditions were similar and showed a fast increasing trend. This section deals specifically with F_{tlmax} response to G_{MOD} in the rock D-P constitutive model under different max conditions. Fixing three ε_{max} at 1.72 × 10^{-3}, 2.58 × 10^{-3}, 3.08 × 10^{-3} and changing G_{MOD} from ±10 % to ±50 % and fitting the corresponding max values were computed and fitted. The results showed that for each fixed max, the maximum rock drilling force showed a linear growth trend as the G_{MOD} increased. When ε_{max} was set at 1.72 × 10^{-3}, F_{tlmax} rose from 6.91 kN to 25.58 kN as G_{MOD} increased from 3.708*10^{-3} MPa to 11.125*10^{-3} MPa, which is about 270.15 % increase. For ε_{max} equal to 2.58 × 10^{-3}, F_{tlmax} increased from 14.90 kN to 46.33 kN, reflecting an increase of approximately 210.99 %. Finally, when ε_{max} reached 3.08 × 10^{-3}, F_{tlmax} grew from 19.93 kN to 55.71 kN, marking an increase of approximately 179.56 %.

Table 2 Fitting results of F_{tlmax} for the variation of G_{MOD} under ε_{max} conditions

Maximum principal strain at failure ε_{max}	Linear fitting results of F_{tlmax} / kN	R^2 (COD) of the linear fitting curve
1.72 × 10^{-3}	F_{tlmax}=-2.710155+2.697241G_{MOD}	0.95111
2.58 × 10^{-3}	F_{tlmax}=-0.370219+4.374242G_{MOD}	0.98208
3.08 × 10^{-3}	F_{tlmax}=3.472635+4.776869G_{MOD}	0.99078

Using the fitting formulas, the value of F_{tlmax} under the corresponding conditions can be calculated more rapidly. Linear fitting of the three curves shown in Table 2 showed a correlation between F_{tlmax} and G_{MOD}, which confirmed the linear growth trend. Increased G_{MOD} increased the stiffness of rock, which increased the propagation speed of stress waves and improved wave impedance matching between the drill bit and rock. This increased impact energy to rock fragmentation work, leading to a linear increase of F_{tlmax}. The parameter ε_{max} defined the ultimate deformation capacity of rock. When ε_{max} was moderate, rock had both ductility and

 https://doi.org/10.64486/m.66.1.9

strength. The impact energy was effectively transmitted, promoting crack propagation through moderate plastic deformation. The parameters ε_{max} and G_{MOD} were related to each other. G_{MOD} affects the growth slope of F_{tlmax}, and ε_{max} determines the baseline value of F_{tlmax}. The slopes of F_{tlmax} growth with respect to G_{MOD}, or sensitivities to G_{MOD}, differed among the investigated conditions, with the highest sensitivity occurring at ε_{max} = 2.58 × 10^{-3} and the lowest sensitivity at ε_{max} = 3.08 × 10^{-3}. Overall, for a given G_{MOD} value, especially at larger G_{MOD} values, F_{tlmax} and ε_{max} had roughly "upward-convex" linear distribution and is shown in Figure 12.

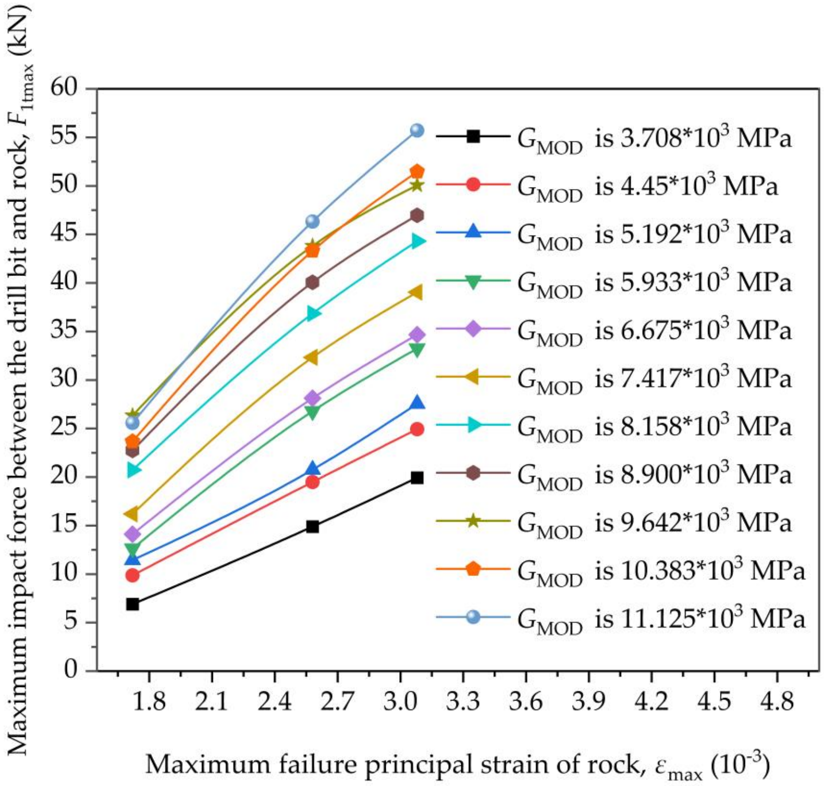

Figure 12. The distribution of F_{tlmax} under different ε_{max} with varying G_{MOD}

5. Conclusion

The statistical numerical sensitivity analysis of rock material parameters led to the following main conclusions for the D–P failure model:

First, mesh-independence verification showed that, for rock element sizes ranging from 0.750 mm to 1.050 mm, the variation in the maximum impact force between the drill bit and the rock remained small (with a change rate below 6.74 %), while an element size of 1.000 mm significantly improved computational efficiency without compromising calculation accuracy.

Second, the maximum impact force between the drill bit and rock, F_{tlmax}, is strongly affected by the elastic shear modulus of rock, G_{MOD}. An increase in G_{MOD} leads to an approximately linear increase in F_{tlmax} because it directly affects rock stiffness and stress-wave velocity. The increase in elastic shear modulus improves wave-impedance matching and energy-transfer efficiency, resulting in a higher drilling force. The maximum principal strain at failure, ε_{max}, which reflects the ultimate deformation capacity of the rock, also has a significant influence. An increase in ε_{max} improves rock ductility, leading to a monotonic increase in drilling force, although the growth rate gradually decreases with increasing strain level. The Poisson ratio of rock, R_{nu}, and rock mass density, r_o, have similar effects on lateral deformation and inertial response, producing a non-monotonic variation in drilling force due to stress-wave reflection and energy coupling effects. The friction angle of rock, P_{HI}, and the dilation angle of rock, P_{SI}, when assigned equal values, have a secondary influence. Their effects are more pronounced within the angle range of 22.5°–40.5° and become more stable beyond this range. Variations in the cohesion value of rock, CVAL, have the weakest influence. In the dynamic impact rock-breaking process, its effect is relatively small, and F_{tlmax} shows only limited variation. The elastic shear modulus

 https://doi.org/10.64486/m.66.1.9

of rock, G_{MOD}, remains the dominant factor influencing F_{tlmax} under different maximum principal strain at failure (ε_{max}) conditions. Together, G_{MOD} and ε_{max} determine both the reference level and the growth rate of F_{tlmax}.

Third, future work should incorporate experimental validation using real lithologies, coupled simulations of rock-breaking sequences involving different drill-bit types, modelling of cuttings formation and removal processes, and environmental factors such as temperature and moisture that may affect the D–P parameters and the maximum impact force between the drill bit and the rock. In addition, the present study does not consider the effects of rock porosity, temperature, or drill-bit wear, nor does it include wear-model analysis. Future research will focus on these aspects through the application of mixed failure criteria, thermo-mechanical coupling, wear models, and related advanced modelling approaches.

Funding

This study was supported by science and technology research key competitive project of Quzhou science and technology bureau (No. 2025K252, No. 2025K249, No. 2023K266, No. 2024K010), the second batch of teaching reform projects of Zhejiang provincial department of education 14th five-year plan (NO. jg20240266, jg20240261), project of the state administration for market regulation (No. 2023MK050), general research project of Zhejiang provincial department of education (No. Y202455816).

References

[1] H. Cheng, H. Fu, L. Zeng, et al., "Mechanical properties and constitutive model of silty mudstone considering drying-wetting cycle path," *Journal of Zhejiang University (Engineering Science)*, vol. 58, no. 9, pp. 1912–1922, 2024. https://doi.org/10.3785/j.issn.1008-973X.2024.09.016

[2] T. Hu, H. Zhou, and Z. Kang, "Transverse isotropic strength criterion and parameter identification method for carbonaceous slate," *Journal of Highway and Transportation Research and Development*, vol. 41, no. 9, pp. 190–197, 2024. https://doi.org/10.3969/j.issn.1002-0268.2024.09.021

[3] C. Huang, "Analysis of influencing factors and parameter optimization of cutting blasting effect in small section roadway of phosphate mine," M.S. thesis, Wuhan University of Science and Technology, Wuhan, China, 2024 (In Chinese). [Online]. Available: https://d.wanfangdata.com.cn/thesis/Ch1UaGVzaXNOZXdTb2xyOVMyMDI2MDUxMjA3Mjk0NxIIWTQzNzQ5MDYaCHFkeXZ5bmRh

[4] Y. Li, "Research on weak-strong discontinuous numerical methods for analysis of progressive failure process in geomaterials," Ph.D. dissertation, Dalian University of Technology, Dalian, China, 2024 (In Chinese). [Online]. Available: https://d.wanfangdata.com.cn/thesis/Ch1UaGVzaXNOZXdTb2xyOVMyMDI2MDUxMjA3Mjk0NxIJRDAzODY1NDY4Gghhem4yMmJzZg%3D%3D

[5] T. Saksala, A. R. Ruiz, S. Bhusare, et al., "Numerical modelling of frictional sliding induced damage and heating effects on rock with an application to Sievers' J-miniature drilling on granite," *International Journal for Numerical and Analytical Methods in Geomechanics*, vol. 49, pp. 2634–2654, 2025. https://doi.org/10.1002/nag.4005

[6] G. Sansyzbekov, A. C. Adoko, and P. M. George, "Thermal damage characterization and modeling in granite samples subjected to heat treatment by leveraging machine learning and experimental data," *Applied Sciences*, vol. 15, no. 11, Art. no. 6328, 2025. https://doi.org/10.3390/app15116328

[7] M. Pressacco, J. J. J. Kangas, and T. Saksala, "Numerical modelling of microwave irradiated rock fracture," *Minerals Engineering*, vol. 203, Art. no. 108318, 2023. https://doi.org/10.1016/j.mineng.2023.108318

[8] X. Wang, Y. Wei, T. Jiang, et al., "Elastic-plastic criterion solution of deep roadway surrounding rock based on intermediate principal stress and Drucker-Prager criterion," *Energy Science & Engineering*, vol. 12, no. 6, pp. 2472–2492, 2024. https://doi.org/10.1002/ese3.1756

[9] H. Liu, J. Liang, Z. Han, et al., "Approximate solution of plastic zone in surrounding rock under three-dimensional stress field based on Drucker-Prager strength criterion," *Journal of Mining Science and Technology*, vol. 9, no. 6, pp. 909–920, 2024. https://doi.org/10.19606/j.cnki.jmst.2024924

[10] Q. Xia, Y. Luo, and X. Wang, "Earth pressure calculation model considering double-shear intermediate principal stress," *Journal of Highway and Transportation Research and Development*, vol. 42, no. 7, pp. 89–98, 2025. https://doi.org/10.3969/j.issn.1002-0268.2025.07.010

[11] Y. Xue, T. Jiao, and B. He, "Research on the mechanism of strain rock burst based on strength and energy theory," *Journal of Engineering Geology*, vol. 33, no. 2, pp. 471–481, 2024. https://doi.org/10.13544/j.cnki.jeg.2024-0059

[12] X. Yuan, H. Liu, and Z. Wang, "Study of elastoplastic damage constitutive model of rocks based on Drucker-Prager criterion," *Rock and Soil Mechanics*, vol. 33, no. 4, pp. 1103–1108, 2012. https://doi.org/10.3969/j.issn.1000-7598.2012.04.021

[13] C. Zang, "Rock breaking simulation and optimization of PDC bit for Jimsar shale formation," *China Petroleum Machinery*, vol. 53, no. 9, pp. 29–36, 2025. https://doi.org/10.12473/CPM.202411063

[14] Q. Zhang, Generalized Three-Dimensional Nonlinear Rock Mass Strength Criterion and Application. Nanjing, China: Southeast University Press, 2023 (In Chinese). [Online]. Available: https://vufind.library.sh.cn/Record/c046cc18-b20c-44f1-8dac-50ce5210020c-1

[15] S. Liu, Q. Dai, S. An, et al., "Analysis of plastic zone and influencing factors of fractured surrounding rock in the arched roadway," *Nonferrous Metals (Mining Section)*, vol. 77, no. 3, pp. 93–100, 2025. https://doi.org/10.20238/j.issn.1671-4172.2025.03.013

[16] H. Zhao, Q. Li, T. Chen, et al., "Research and application of air DTH hammer drilling technology for deep geothermal well in Guizhou carbonate formation," *Exploration Engineering (Rock & Soil Drilling and Tunneling)*, vol. 44, no. 2, pp. 37–42, 2017. https://doi.org/10.3969/j.issn.1672-7428.2017.02.008

[17] C. Zhao, X. Yang, C. Zhang, et al., "Investigation on applicability of common failure criteria considering intermediate principal stress," *Chinese Journal of Rock Mechanics and Engineering*, vol. 30, no. 2, pp. 327–334, 2011 (In Chinese). [Online]. Available: https://d.wanfangdata.com.cn/periodical/CihQZXJpb2RpY2FsQ0hJU29scjkyMDI2MDYxMDIwMjYwNjEwMTYxMjM4EhJ5c2x4eWdjeGIyMDExMDIwMTUaCDgyZ2Qycm5w

[18] D. Li, Z. Huang, H. Lin, et al., "Influence of drilling incidence angle on the drilling force distribution of pneumatic impactor," *Scientific Reports*, vol. 15, no. 1, Art. no. 2098, 2025. https://doi.org/10.1038/s41598-025-86071-2

[19] D. Li, L. Tong, Z. Huang, et al., "Numerical analysis on the drilling force of pneumatic impactors under different working conditions and structural parameters," *Scientific Reports*, vol. 15, no. 1, Art. no. 33405, 2025. https://doi.org/10.1038/s41598-025-18751-y

[20] D. Han, "Study on dynamic fracture capabilities of rock materials and numerical simulation," Ph.D. dissertation, Anhui University of Science and Technology, Huainan, China, 2014 (In Chinese). https://doi.org/10.7666/d.Y2696870

[21] C. Bi, "Calibration of HJC constitutive parameters of Huashan granite and its blasting damage numerical simulation," M.S. thesis, Hefei University of Technology, Hefei, China, 2018 (In Chinese). https://doi.org/10.7666/d.Y3386106

[22] L. Wen, X. Li, Q. Wu, et al., "Study on parameters of Holmquist-Johnson-Cook model for granite porphyry," *Chinese Journal of Computational Mechanics*, vol. 33, no. 5, pp. 725–731, 2016. https://doi.org/10.7511/jslx201605011